Vibration Sensing using Doppler-modulated Chipless RFID Tags

Ashkan Azarfar, Nicolas Barbot, Etienne Perret

Vibration Sensing using Doppler-modulated Chipless RFID Tags

Ashkan Azarfar, Nicolas Barbot, Etienne Perret
Univ. Grenoble Alpes, Grenoble INP, LCIS, F-26000 Valence, France
ashkan.azarfar@lcis.grenoble-inp.fr

***Abstract*— The paper describes how chipless tags attached to non-metal vibrating objects can be utilized to sense the frequency and amplitude of mm-vibration without any calibration process, and to identify the tag from large distances in low microwave frequency band. It is demonstrated that micro-Doppler harmonics induced by vibrating high-resonant scatterers are more detectable than those induced by the vibrating object itself while the scatterers provide great area efficiency. Presented methods for vibration sensing and identification are experimentally validated for sub-millimeter vibrations at distances up to 8 meters.**

***Keywords*— Chipless Radio Frequency IDentification (RFID), Doppler effect, Resonant Scatterer, Vibration sensing.**

I. Introduction

In microwave and millimeter-wave vibration sensing based on phase interferometry, the frequency and amplitude of vibration can be characterized based on micro-Doppler harmonics which appear in the backscattered signals [1]. In most applications like healthcare monitoring [2], only the vibration frequency is detected by using first micro-Doppler harmonic. However, the vibration amplitude, without any calibration process, can be determined only if the higher order harmonics are considered too [3]. Millimeter-wave radars due to their shorter operating wavelength provide better resolution and a higher number of detectable harmonics which facilitate the amplitude detection. Nevertheless, it should be noted that other key parameters as Radar Cross Section (RCS) of the vibrating target and the path-loss at operating frequency will also affect the vibration sensing process. For example, the reflection coefficient of the human body is about only 40% in mm-wave band [4] which causes to degrade the vital signs sensing performance at large distances. This effect can be compensated by using high-gain antennas whereas misalignment constraints appears as in optical methods. Apart from this, the main challenge for mm-wave radars raises in scenarios in which the radar should detect the vibrating target between other vibrating objects with similar characteristics (e.g. two humans). As a solution, at low microwave frequencies, this issue can be effectively alleviated by using RF tags attached to the target which make it distinguishable. In [5], a passive RF harmonic tag has been utilized to robustly monitor the respiration rate in the presence of other moving objects at one meter range without identification capability. Moreover, chipless RFID tags have been utilized, but not based on interferometry, for displacement sensing in [6] with limited read range of 40 cm. However, in [7] it has been proved that moving chipless tags, thanks to the micro-Doppler effect, can be read at larger distances up to several meters.

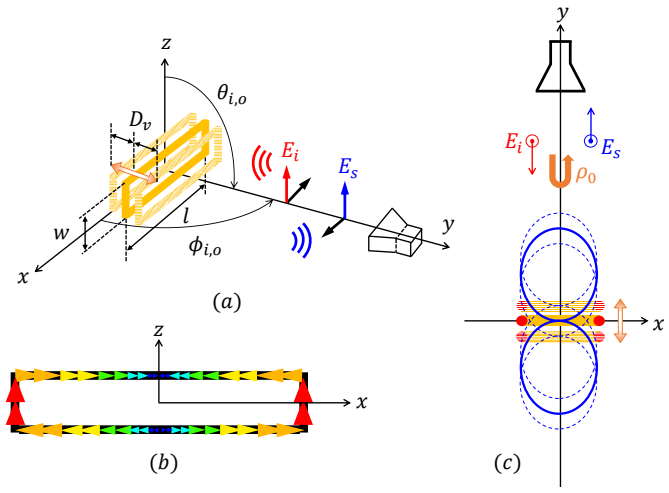

Fig. 1. (a) Backscattering from vibrating rectangular loop in normal direction. (b) Current distribution on the loop in fundamental resonant mode. (c) Reradiation pattern of the loop during vibration.

In this paper low-cost RF chipless tags consisting of high-resonant scatterers are used to sense vibration parameters (frequency and mm-range amplitude) with identification capability at a relatively long range. As the key advantage, it is demonstrated that the attached chipless tag can provide more detectable micro-Doppler harmonics compared to the vibrating object itself, with great area efficiency.

II. Theory and Methodology

A. Backscattering from vibrating rectangular loop

Fig. 1(a) shows a rectangular loop of wire with the length of l (in x-direction), width of w (in z-direction), and wire radius of a which is vibrating in y-direction. The vibration is assumed to be single tone with amplitude of D_v and frequency of f_v which can be expressed as $D_v \sin(2\pi f_v t)$. The far-field radiation of an antenna, as a z-polarized plane wave, normally impinges the vibrating loop at (θ_i=ϕ_i=$\pi/2$) and the scattered field is captured by the same antenna at (θ_o=ϕ_o=$\pi/2$). Thus, the incident electric field at the carrier frequency of f_c can be written as $\vec{E_i}(\vec{r})$=$E_0\, e^{jky}\, \hat{z}$ where k=$2\pi f_c/c_0$=$2\pi/\lambda$ and c_0 is the free-space light velocity. Normal incident z-polarized field will excite the fundamental resonant mode of the loop (l=$\lambda/2$) with current distribution depicted in Fig. 1(b). For $w \ll l$, only the two small sides of the loop with in-phase currents will contribute in reradiation with a normalized

reradiation pattern of $\sin\theta\cos(\frac{\pi}{2}\cos\phi)$. As it is shown in Fig. 1(c), for normal observation angle (θ_o=ϕ_o=$\pi/2$), the reradiation intensity of the loop does not change with respect to the antenna during the vibration. Therefore, the complex envelope of the backscattered field can be safely written based on the general micro-Doppler formulation [1] as

$$\vec{E}_s(\vec{r},t) = \rho_0(f_c)\, E_0 \frac{e^{-jky}}{2\sqrt{\pi}y}\, e^{j2kD_v \sin(2\pi f_v t)}\, \hat{z} \qquad (1)$$

where $\rho_0(f_c)$ is a complex scattering coefficient linked to the RCS of the loop at the normal direction as $|\rho_0(f_c)|^2 = \sigma(f_c)$. The spectral representation of (1) can be derived as

$$\vec{\mathbf{E}}_s(\vec{r},f) = \rho_0(f_c)\, E_0 \frac{e^{-jky}}{2\sqrt{\pi}y} \sum_{n=-\infty}^{+\infty} J_n(\beta)\delta(f-nf_v)\, \hat{z} \qquad (2)$$

where β=$4\pi D_v/\lambda$ and $J_n(\beta)$ is the first kind Bessel function of order n which defines the amplitude of the n-th micro-Doppler harmonic. When the loop scatterer is attached to a non-metalic vibrating object with physical area of A_o seen by antenna, at the resonance (l=$\lambda/2$), the RCS level of the loop with physical area of A=wl≪A_o can be much larger than that of the vibrating object. This point proves that loop resonators can be utilized to detect vibration-induced micro-Doppler harmonics from larger distances with significant area efficiency. Moreover, it plays an important role for mm-vibration sensing at several-GHz frequencies where β value is quite small (β<0.5).

B. Vibration parameters sensing

After coherent reception, the Power Spectral Density (PSD) of the complex baseband received signal $S_r(f)$ will contain the same non-zero frequency components as (2) located at $\pm f_v, \pm 2f_v, ...$ with associated amplitudes of $C_{\pm1}, C_{\pm2}, ...$ such that $|C_{-n}|$=$|C_{+n}|$ for n=$1,2,....$ The vibration frequency f_v is readily obtained from the first harmonic (n=1) whereas the amplitude of the vibration, without using any calibration process, can be determined only if the absolute harmonics ratios ($|C_n|/|C_m|$, n≠m>1) are considered [3]. Accordingly, a least-square (LS) estimator based on the successive harmonics ratio is introduced as

$$\hat{\beta}_s = \min\left(\sum_{n=1}^{N-1}\left|\frac{|J_n(\beta)|}{|J_{n+1}(\beta)|} - \frac{|C_n|}{|C_{n+1}|}\right|^2\right) \qquad (3)$$

to obtain the solution $\hat{\beta}_s$ and consequently the vibration amplitude D_v where N is the order of the last detectable harmonic. Contrary to detection method presented by [3], the proposed estimator in (3) can provide a unique solution for vibration amplitude while β<0.5 and when only a limited number of harmonics are detectable (N<5) which happens for mm-vibration sensing at several-GHz frequencies.

C. Vibrating object identification based on differential RCS

When a multi-loop chipless tag is attached to the vibrating object, besides enhancing the detection range, it provides identification capability which can be used to distinguish the target from other moving objects. The identification process can be done based on differential RCS of the moving chipless tag [7]. Similarly as [7], differential RCS of the vibrating loop (σ_d) is associated to the total modulated power around the carrier frequency and can be calculated based on the backscattered field as

$$\sigma_d(f_c) = \lim_{y\to\infty} 4\pi y^2 \frac{\int_B |\vec{\mathbf{E}}_s(\vec{r},f)|^2\, df}{|E_0|^2} = \sigma(f_c)[1-J_0^2(\beta)] \qquad (4)$$

where $B = (-\infty,-\epsilon]\cup[\epsilon,+\infty)$ is zero-excluded integration bandwidth with infinitesimal $\epsilon > 0$. Equation (4) clearly shows that differential RCS of the vibrating loop is directly related to its highly-resonant RCS which can be utilized to identify multi-loop tags during the vibration.

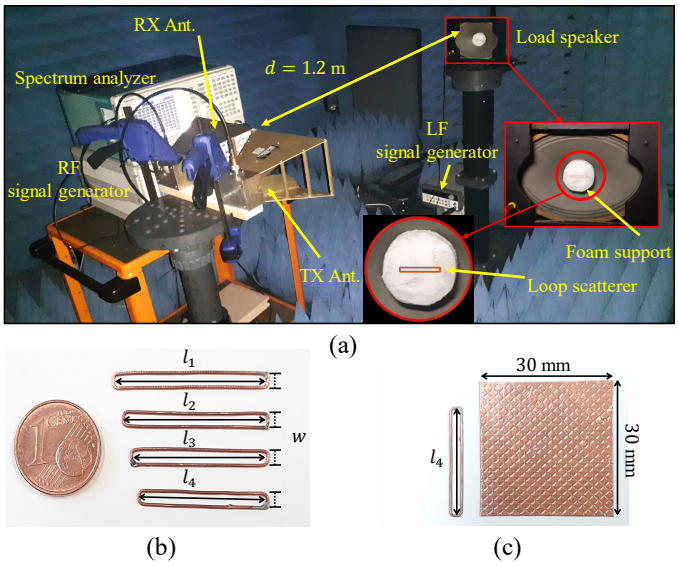

Fig. 2. (a) Measurement bench used for vibration sensing. (b) Fabricated loop scatterers as loop No.1 to 4. (c) Copper plate in compare with loop No.4.

III. Results and Discussion

A. Measurement Bench

The measurement bench is presented in Fig. 2(a) and is composed of a VNA (HP 8720D), used as RF signal generator in CW mode, and a spectrum analyzer (Tektronix RSA3408A) which are respectively connected to TX and RX antennas (A.H. Systems SAS-571). The antennas are closely positioned tending to the monostatic configuration compatible with the model. A simple loudspeaker with an attached foam support has been employed to realize the single tone one-dimensional vibration. The speaker is normally faced to the antennas and vertically aligned with them. An LF signal generator is used to feed sinusoidal voltage (V_s=$V_0\sin 2\pi f_v t$) into the speaker. According to mechanical behaviour of the speaker, the vibration frequency has been set to 68 Hz to provide sensible vibration while its amplitude can be modified by varying V_0. The speaker is placed at $d = 1.2$ m distance from the antennas to fulfill the far-field radiation condition. The carrier frequency (f_c) can be set in-between 4.5 and 6 GHz and the output power

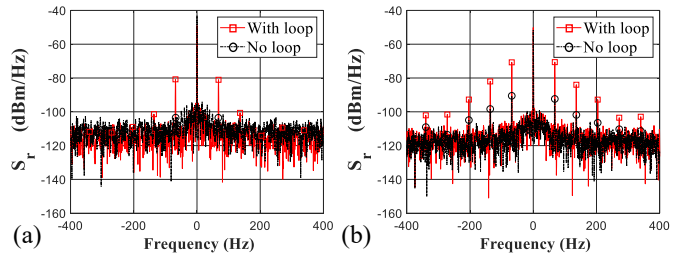

Fig. 3. Measured PSD of backscattering from the speaker when loop No.4 is attached and when the loop is absent (a) for V_0=1.25 V (b) for V_0=5 V.

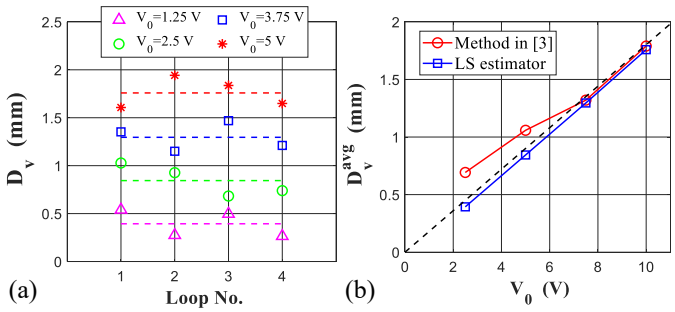

Fig. 4. (a) Estimated vibration amplitude for four voltage levels feeded to speaker using loop No.1 to 4. Average value at each level is shown in dashed line. (b) Averaged estimated amplitude as a function of voltage. Straight line is depicted in black dashed line for comparison.

(P_t) is 0 dBm. The spectrum analyzer acquires the received signal over a span of 800 Hz around each carrier frequency while it has been coherent with the VNA using 10 MHz common reference signal. It is worth mentioning that although due to the mechanical constraints of the speaker the vibration frequency is selected as 68 Hz, the measurements can be accurately done even at vibration frequencies less than 1 Hz as long as the transmitter and receiver are coherent. Rectangular loops considered in this paper are shown in Fig. 2(b). Four loops namely loop No.1, 2, 3, and 4 have been fabricated from pieces of 500 μm copper wire with defined lengths, which are formed in the rectangular shape using a 2mm-thick metal plate and finally are soldered in a corner point. The fabricated rectangular loops No.1 to 4 have respective lengths of l_1=28.5 mm, l_2=27 mm, l_3=25.5 mm, and l_4=24 mm, and a width of w = 2 mm. Using a standard RCS measurement procedure, the fundamental resonance frequency of the loops No.1, 2, 3, and 4 has been measured as 4.78, 5.01, 5.37, and 5.78 GHz respectively.

B. Vibration sensing and vibrating tag identification

The vibration sensing is examined for V_0=1.25, 2.5, 3.75, and 5 V while each loop is mounted on the foam support and f_c has been set at the corresponding resonance frequency. For example, the measured backscattered PSD associated to the loop No.4 when V_0 = 1.25 V and 5 V are presented in Fig. 3(a) and (b) respectively, which clearly show detectable micro-Doppler harmonics compared to when the loop is absent. The vibration frequency is accurately measured as

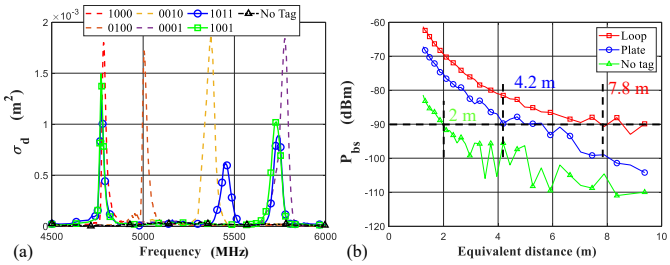

Fig. 5. (a) Calculated differential RCS for designed chipless tags. IDs are assigned such that loop No.1 and loop No.4 corresponds to most and least significant bit respectively. (b) Vibration sensing read range for speaker itself and when loop No.4 or copper plate is attached to it [see Fig. 2(c)].

68.2 Hz using the first harmonic. Based on (3) with N=3, the vibration amplitude has been estimated at each voltage level by using loops No.1 to 4 and the results are shown in Fig. 4(a). The average estimated amplitude as a function of V_0 is presented in Fig. 4(b). Since the speaker, as a mechanical system, behaves linearly for small exciting forces, the perfect linear variation of the estimated amplitude versus V_0 proves the validity of the results and good performance of the proposed estimator. The results obtained from the method presented in [3] (detection based on only one harmonic ratio as $|J_3|/|J_1|$) is also depicted in Fig. 4(b) which shows better performance for LS estimator. For V_0=5 V, the calculated differential RCS of the vibrating loops as a function of carrier frequency (f_c ; 4500:10:6000 MHz) are presented in Fig. 5(a). At each f_c, the differential backscattered power $P_{bs\,d}$ (i.e., power associated to the side bands) has been obtained based on the measured PSD and σ_d is calculated by $\sigma_d(f_c)$=$[(4\pi)^3 d^4 P_{bs\,d}]/[P_t G^2 \lambda^2]$ where G is the antennas gain. The identification process based on σ_d is demonstrated by the observed peaks at the resonance frequency of each loop, which also validates (4). Moreover, the calculated σ_d for two multi-resonator tags are added in Fig. 5(a) to demonstrate the identification capability which is an advantage of the proposed idea compared to [5] in multi-object scenarios.

C. Read Range

The advantage of using high-resonant scatterers to enhance vibration sensing range is investigated experimentally when V_0=5 V. The $P_{bs\,d}$ is measured for three cases as 1) speaker itself, 2) speaker attached with loop No.4, and 3) speaker attached with the copper plate shown in Fig. 2(c), at the same frequency of 5.78 GHz. To obtain the maximum achievable read range for each case, at the fixed distance of d=1.2 m, $P_{bs\,d}$ has been measured as a function of P_t ; -30:1:5 dBm. Afterwards, for each P_t value, the equivalent distance is determined by assuming a fixed transmitted power of 5 dBm. The measured $P_{bs\,d}$ as a function of equivalent distance is presented in Fig. 5(b) for the three cases. Considering a detection threshold of -90 dBm, the vibration can be sensed by using the loop at distances of at least four and two times of what can be reached respectively without any loop and with the plate.

IV. Conclusion

Chipless RFID tags consist of high-resonant rectangular loops have been employed for mm-vibration sensing at several-GHz frequencies from large distances. An analytical model has been presented for backscattering from the vibrating loop, and a vibration amplitude estimator based on micro-Doppler harmonics ratio has been introduced. Performance of the amplitude estimator and the identification capability based on differential RCS have been verified in measurements for mm-vibrations. At best, at least in 3 m range, a $400\,\mu$m vibration amplitude can be measured at 5.78 GHz while the transmitted power (0 dBm) is much smaller than what is licensed for 5.8 GHz ISM band (30 dBm).

Acknowledgment

This work was supported by the European Research Council (ERC) through the European Union's Horizon 2020 Research and Innovation Program (ScattererID) under Grant N° 772539. The authors are also thankful towards Ms. Nathalie Franck for her help in proofreading the paper.

References

[1] V. C. Chen, F. Li, S. . Ho, and H. Wechsler, "Micro-Doppler effect in radar: phenomenon, model, and simulation study," *IEEE Trans. Aerosp. Electron. Syst.*, vol. 42, no. 1, pp. 2–21, Jan. 2006.

[2] C. Li, V. M. Lubecke, O. Boric-Lubecke, and J. Lin, "A review on recent advances in Doppler radar sensors for noncontact healthcare monitoring," *IEEE Trans. Microw. Theory Techn.*, vol. 61, no. 5, pp. 2046–2060, 2013.

[3] C. Li and J. Lin, "Non-contact measurement of periodic movements by a 22-40GHz radar sensor using nonlinear phase modulation," in *2007 IEEE MTT-S Int. Microw. Symp. Dig.* IEEE, 2007, pp. 579–582.

[4] Y. Feldman *et al.*, "The electromagnetic response of human skin in the millimetre and submillimetre wave range," *Physics in Medicine & Biology*, vol. 54, no. 11, p. 3341, 2009.

[5] A. Singh and V. M. Lubecke, "Respiratory monitoring and clutter rejection using a CW doppler radar with passive RF tags," *IEEE Sensors Journal*, vol. 12, no. 3, pp. 558–565, 2011.

[6] E. Perret, "Displacement sensor based on radar cross-polarization measurements," *IEEE Trans. Microw. Theory Techn.*, vol. 65, no. 3, pp. 955–966, 2017.

[7] A. Azarfar, N. Barbot, and E. Perret, "Towards chipless RFID technology based on micro-Doppler effect for long range applications," in *2021 IEEE MTT-S Int. Microw. Symp. Dig.* IEEE, 2021, pp. 819–822.